Earth and Space Science

RESEARCH ARTICLE
10.1029/2023EA002954

Impact of Forbush Decreases and Geomagnetic Storms on the Atmospheric Ozone Profiles

Natalya Kilifarska[1] **and Klaudio Peqini**[2]

[1]Climate, Atmosphere and Water Research Institute, Bulgarian Academy of Sciences, Sofia, Bulgaria, [2]Department of Physics, Faculty of Natural Sciences, University of Tirana, Tirana, Albania

Key Points:

- The response of ozone profile to the reduced cosmic ray intensity (known as Forbush decrease [FD]) is investigated
- We found that atmospheric ozone beneath its maximum is reduced in periods of FDs
- This result is an indirect confirmation of the existence of secondary source of ozone in the lower stratosphere

Correspondence to:

N. Kilifarska,
natalyakilifarska@gmail.com;
nkilifarska@cawri.bas.bg

Citation:

Kilifarska, N., & Peqini, K. (2023). Impact of Forbush decreases and geomagnetic storms on the atmospheric ozone profiles. *Earth and Space Science*, *10*, e2023EA002954. https://doi.org/10.1029/2023EA002954

Received 28 MAR 2023
Accepted 10 JUN 2023

Author Contributions:

Conceptualization: Natalya Kilifarska
Data curation: Natalya Kilifarska
Formal analysis: Klaudio Peqini
Funding acquisition: Natalya Kilifarska
Investigation: Natalya Kilifarska, Klaudio Peqini
Methodology: Natalya Kilifarska
Resources: Natalya Kilifarska, Klaudio Peqini
Validation: Klaudio Peqini
Writing – original draft: Natalya Kilifarska
Writing – review & editing: Natalya Kilifarska, Klaudio Peqini

Abstract The sensitivity of atmospheric ozone to geomagnetic storms and reduced cosmic rays' (CRs) intensity (called Forbush decrease [FD]) has been noticed for many years. However, it is still unclear what the factors affecting ozone density are—whether these are the complex changes induced by geomagnetic storms in the upper atmosphere and ionosphere, or it is the severe reduction of CRs accessing Earth's lower atmosphere. Analyzing two strong geomagnetic storms, accompanied by FDs, and another FD occurred in geomagnetically quiet conditions, we conclude that observed ozone changes support the idea about the existence of an additional source of ozone in the lower stratosphere. The ion-molecular reactions of catalytic ozone production are initiated by secondary ionization, produced by cosmic radiation at these levels. This conclusion is supported by the fact that the strongest ozone depletion beneath its maximum is found in regions with the severest reduction of CR flux. Moreover, the time delay of ozone response (~2 days), is short enough to be attributed to changes in circulation. In addition, we have examined the changes in the sea level pressure during the analyzed events and found out that the surface pressure follows dynamically the spatial pattern of the ozone changes, forced by the reduced amount of precipitating energetic particles in the atmosphere.

Plain Language Summary Theoretical estimates of the efficiency of the lower stratospheric ion-molecular reactions suggest an existence of another source of ozone (different from the well-known photo-dissociation mechanism). The conditions necessary for activation of autocatalytic ozone production require: (a) increased density of the low energy electrons (naturally produced at these levels by cosmic rays) and (b) reduced amount of water molecules above the tropopause. The short-lasting periods of a significantly decreased cosmic radiation—known as Forbush decreases (FDs)—provide a good opportunity for testing the above hypothesis. In this paper, we have compared the spatial distribution of three different FDs with changes in the lower stratospheric ozone density. We show that the strongest ozone depletion (beneath the ozone layer maximum) coincides very well with the largest magnitude of the FD. The time delay of ozone response to the applied forcing is too short, so the ozone depletion could not be attributed to the stratospheric circulations (as usually done). This result could be interpreted as an indirect confirmation of the importance of energetic particles, precipitating in the Earth's atmosphere, for the spatial-temporal variability of the lower stratospheric ozone density.

1. Introduction

The geomagnetic field distortions, known as geomagnetic storms, are forced by a shockwave—propagating through the interplanetary medium after the solar flares, coronal mass ejection, high-speed streams, or other active processes on the Sun. The imposed magnetic irregularities reflect or scatter a part of galactic cosmic rays (CRs) traveling through the heliosphere. As a result, the geomagnetic storms are usually accompanied by a significant decrease of the flux of highly energetic particles reaching the Earth. Such short-lasting decreases of CRs' intensity are known as Forbush decreases (FDs). However, FDs are observed also without the occurrence of geomagnetic disturbances. These two events impact the atmospheric chemical composition—and particularly the ozone. Moreover, it is still unclear whether the effect of geomagnetic storm differs from that of the FD, and if so—what are the mechanisms of such an influence on the ozone.

Statistical evidence for geomagnetic imprint on the ozone density has been found long ago. Most of the studies, examining geomagnetic storms-ozone relation, are focused on the total ozone density response. The reported results, however, are quite contradictive. Some of the authors claimed ozone depletion during or short after the onset of geomagnetic storms (Bekoryukov et al., 1976; Bhargawa et al., 2019; Storini, 2001). Others report

about an opposite effect—that is, about an enhancement of the total ozone density (Laštovička & Mlch, 1999; Shirochkov & Nagurny, 1992). A third group of authors found out a diverse ozone response with a significant altitudinal, latitudinal, longitudinal, and temporal variability (Belinskaya et al., 2001; Okoro et al., 2022; Tassev et al., 2003).

The appearance of FD could vary with respect to the beginning of geomagnetic storm. Moreover, a significant difference in the FD's onset is a typical for the non-simultaneous FDs (Oh & Yi, 2009). So, attempts to differentiate the effects of FD from that of the geomagnetic storm are well appreciated. Putting the focus on the FD onset, Fedulina (1998) found out that ozone responds to FDs with a well-pronounced depletion in both—total ozone density and ozone profile near the Regener-Pfotzer maximum (i.e., the layer of secondary ionization, created by CRs in the lower stratosphere).

A step forward in disentangling the Forbush and geomagnetic storm effects is made in Laštovička and Križan (2005). Despite the reduced amount of single events, that is, FDs without geomagnetic storms and vice versa, the authors conclude that the FDs are of decisive importance for geomagnetic storms' impact on the total ozone density.

Another hypothesis relates the geomagnetic storm influence on ozone to the imposed changes on atmospheric circulation. According to Bucha and Bucha (1998), the storm-induced upper atmospheric circulation propagates from the thermosphere downward to the stratosphere and troposphere. Other hypothesis suggests, however, that changes in stratosphere-troposphere circulations are determined locally, by changes in atmospheric transparency (Veretenenko & Ogurtsov, 2012). Thus, up to date, there is not an accepted mechanism for geomagnetic storm influence on the circulation in the stratosphere and troposphere.

It is worth reminding that sudden decreases of geomagnetic field, during magnetic storms, have dramatic effects mainly on the upper atmospheric layers—the thermosphere and ionosphere. FDs of CR intensity, on the other side, affect mainly the lower atmosphere, and the mechanism of such an influence on the ozone was revealed recently (Kilifarska, 2013). According to the author, the secondary ionization produced by CR in the lower stratosphere activates an autocatalytic cycle of ozone production. Its efficiency depends on the amount of low-energy electrons, available in the Regener-Pfotzer maximum, as well as on the dryness of the atmosphere. Consequently, the reduced intensity of CR flux should be projected as ozone depletion in the lower stratosphere.

This study provides an attempt to differentiate between geomagnetic storm and FD impacts on the ozone profile, in different regions of the Northern Hemisphere. Two geomagnetic storms have been analyzed—the first occurred on 6 November 2001 (with a maximal Dst index −292 nT), and the second one—on 24 November (max. Dst = −221 nT). Both storms are accompanied by strong FDs—for example, according to the IZMIRAN's catalog with a magnitude of 13.3% and 9.8% decrease of 10 GV energetic particles' intensity (Belov et al., 2018). The magnitude of FDs is corrected for the magnetospheric effect by using Dst index. These FDs appear simultaneously in all neutron monitors. Another FD has been analyzed, which is not a geomagnetic storm companion. It has been a non-simultaneous event with an onset in various days between 31 December 2001 and 3 January 2002.

2. Data and Methods

Daily values of atmospheric ozone and sea level pressure have been taken from ECMWF ERA-Interim analysis (Simmons et al., 2006), for the period November 2001 to January 2002. The deviations of daily values from their monthly means (called furthermore *anomalies*) have been calculated in a regular grid with 5° step in latitude and longitude. These values have been used for creation of maps, illustrating the spatial distribution of ozone and pressure response to the applied external forcing.

Energetic particles reaching the ground-based neutron monitors are subject to magnetic lensing (Kilifarska et al., 2020), due to the geomagnetic field's spatial heterogeneity. So the irregular distribution of the high energy particles accessing the ground level has been illustrated by maps of the FD magnitude over the Northern Hemisphere. The maps have been created by data taken from the global network of neutron monitors, available at NMDB portal: http://www01.nmdb.eu, and from the IZMIRAN's database, available at: http://cr0.izmiran.ru/common/links.htm. All data are corrected for pressure variability and detectors' efficiency. The FD magnitude is calculated as a relative deviation of daily values from their monthly means, in percentage, for each measurement point.

3. Results

3.1. Depletion of Near-Surface Energetic Particles During FDs

The spatial heterogeneity of geomagnetic field suggests that energetic particles reaching the lower atmosphere are also unevenly distributed over the globe (Kilifarska, Bakhmutov, & Melnyk, 2022). To reveal any differences in ozone response to depleted particles' flux during geomagnetic storms and/or FDs, we have to compare regions with different particles' intensity. Here, it is worth to remind that ozone is sensitive not only to the primary CRs, but also to the secondary ionization created by them in the lower atmosphere, known as Regener-Pfotzer maximum (Kilifarska et al., 2020). Consequently, the information about the particles accessing the lower atmospheric levels—provided by the ground-based neutron monitors and muon telescopes—is of special importance for this investigation. Data from 30 neutron monitors in the Northern Hemisphere have been used for creation of maps of the maximal FD amplitude, obtained for each of the examined events. A list with neutron monitors' coordinates and the magnitude of detected FDs are shown in Table 1.

Figure 1 illustrates, that the spatial distributions of the particles' fluxes depletion, during both geomagnetic storms in November 2001, are very similar—with two main regions of strongest reduction centered over the North America, and the Scandinavia–Eastern Europe. The distribution of FD during the third event, however, is quite different (see the bottom panel of Figure 1).

The most impressive in Figure 1 is the longitudinal variations of particles' flux accessing the lower atmosphere. This feature, as described in Kilifarska et al. (2020) should be attributed to the longitudinal gradient and hemispherical asymmetry of geomagnetic field. Unlike the polar region, where energetic particles arrive along the open magnetic field lines, the extratropical and tropical regions are influenced generally by particles trapped in the Earth's radiation belts. These particles are subject to geomagnetic lensing in the lowest part of their trajectories, in the two main regions having a positive azimuthal geomagnetic gradient. The mechanism of particle's lensing could be briefly summarized as follow: when trapped by geomagnetic field, charged particles are separated and protons become drifting westward, while electrons—eastward. The particles' drift velocity depends on their sign, the magnetic gradient, and the magnetic lines' curvature via the formula:

$$v_{drift} = \frac{m}{q \cdot B^2}\left(v_{\perp}^2 \frac{\mathbf{B} \times \nabla \mathbf{B}}{2\mathbf{B}} + v_{II}^2 \frac{\rho \times \mathbf{B}}{\rho^2}\right) \quad (1)$$

where **B** is the magnetic vector, **ρ** is the radius of the geomagnetic lines curvature, v_{II} and $v_{\perp}$ are projections of particle's velocities parallel and perpendicular to geomagnetic field line, q and m are particle's charge and mass, respectively.

Equation 1 shows that the drift velocity component (related to the longitudinal gradient of geomagnetic field—the first term on the right side of Equation 1) is higher in regions with stronger positive azimuthal gradient than in regions with a small one. Moreover, in regions with a negative gradient, the overall westward drift of protons (induced by the geomagnetic field curvature, i.e., the second term in Equation 1) is reduced by the oppositely directed component related to the longitudinal geomagnetic gradient (the first term in Equation 1). Consequently, the bidirectional drift of protons and electrons in the geomagnetic field is much faster in regions with positive azimuthal gradient, and correspondingly the created electric field is much stronger. The latter will intensively expel the charged particles outside the magnetic trap, through the imposed (**E**x**B**)/B^2 drift. Furthermore, these particles interact with the atmospheric constituents creating secondary electrons, ions, and nuclear products. This raises the ionization of the lower atmosphere and correspondingly the neutron monitors' counting rates. Oppositely, the weaker drift velocity in regions with negative longitudinal gradient generates weaker electric field, which is able to expel only a few particles from the geomagnetic trap.

It is worth to remind that the couple of geomagnetic storm and FD appears most frequently as a subsequent result of coronal mass ejection from the Sun. The erupted hot, magnetized plasma, and its shock wave, move through the interplanetary space and interact with galactic CRs in the heliosphere—scattering or reflecting them. When the shock structures of solar wind splash the Earth, they compress the magnetopause toward the Earth, forcing intensification of magnetopause electric currents. The latter in turn raises abruptly the horizontal geomagnetic field. This marks the *initial phase* of geomagnetic disturbance, known as sudden commencement.

Furthermore, if the direction of interplanetary magnetic irregularity is opposite to the direction of Earth's magnetic field, then starts the process of its reconnection to geomagnetic field. It is accompanied by a deep

Earth and Space Science
10.1029/2023EA002954

Table 1
List of Neutron Monitors With Their Codes, Geographic Coordinates, Geomagnetic Rigidity, Elevation Above Sea Level, and Maximal Forbush Decrease Magnitude, Determined for All Three Events

NM code	Lat. (deg)	Long (deg)	Rigidity (GV)	Alt (m)	Ampl. FD 6–7 November 2001 (%)	Ampl. FD 25 November 2001 (%)	Ampl. FD 31 December 2001 to 3 January 2002 (%)
THUL	76.5	−68.7	0.3	26	−4.17	−5.37	−3.68
NRLK	69.26	88.05	0.63	0	−3.81	−4.97	−3.1
INVK	68.36	−133.72	0.3	21	−3.8	−4.78	−4.15
APTY	67.57	33.39	0.65	181	−3.95	−5.95	−4.26
OULU	65.05	25.47	0.81	15	−4.05	−5.76	−4.66
YKTS	61.99	129.7	1.65	105	−3.25	−5.04	−3.19
MGDN	60.04	151.05	2.1	220	−3.54	−6.24	−4.01
FRSM	60.02	−111.93	0.3	180	−3.08	−4.75	−4.9
NAIN	56.55	−61.68	0.3	46	−1.86	−5.87	−4.66
MOSC	55.47	37.32	2.43	200	−3.5	−5.61	−4.84
PWNK	54.98	−85.44	0.3	53	−5.79	−5.48	−4.06
KIEL	54.34	10.12	2.36	54	−3.55	−5.64	−3.79
IRKT	52.47	104.03	3.64	435	−3.42	−5.14	−2.79
CALG	51.08	−114.13	1.08	1,123	−4.72	−6.74	−3.12
DRBS	50.1	4.59	3.18	225	−1.83	−3.87	−5.65
LMKS	49.2	20.22	3.84	2,634	−2.53	−5.32	−5.52
JUNG	46.55	7.98	4.49	3,475	−3.03	−5.22	−4.35
AATB	43.04	76.94	6.69	3,340	−1.83	−4.1	−3.96
ROME	41.86	12.47	6.27	0	−1.96	−3.39	−3.38
NANM	40.37	44.25	7.1	2,000	−0.1	−3.99	−4.72
ARNM	40.47	47.44	7.1	3,200	−4.05	−5.76	−4.66
NEWK	39.68	75.75	2.4	50	−3.24	−5.54	−3.44
BEIJ	39.9	116.41	10	48	−0.13	−4.01	−2.91
ATHN	37.97	23.78	8.53	260	−1.21	−1.9	−3.86
ESOI	33.3	35.8	10.75	2,055	−0.64	−2.67	−3.42
TIBT	30.11	90.56	14.1	4,300	−1.1	−2.96	−2.7
Haleakala	20.71	−156.93	11.5	3,052	−0.41	−1.85	−3.63
MXCO	19.8	−99.18	8.28	2,274	−1.63	−3.28	−3.66

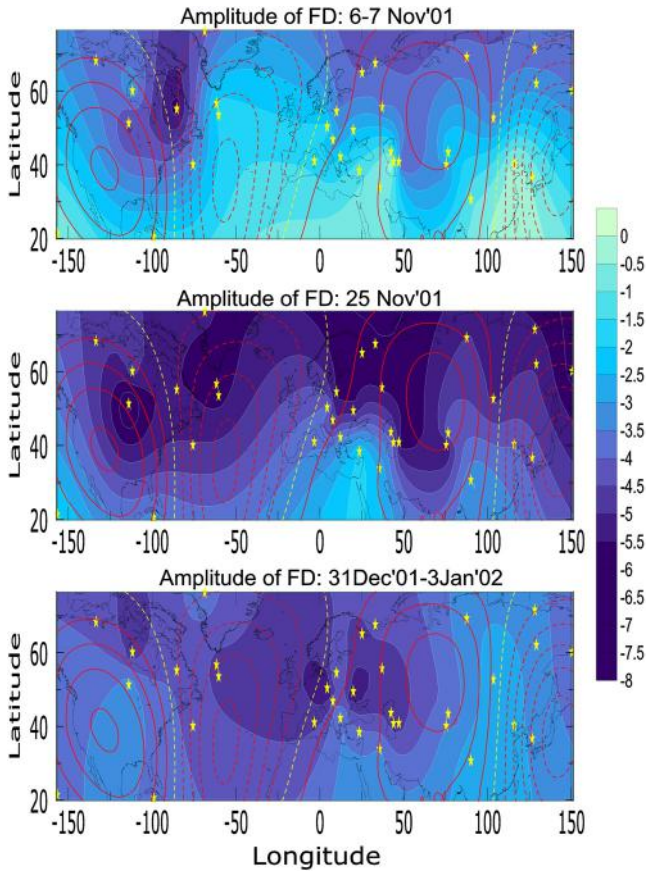

Figure 1. Two upper panels present the spatial distribution of Forbush decrease (FD) magnitude, constructed from a network of 30 neutron monitors' measurements in the Northern Hemisphere, during geomagnetic storms occurred on 6 and 24 November 2001. The bottom panel shows the depletion of particles' intensity corresponding to the FD without geomagnetic storm, observed in the period: 31 December 2001 to 3 January 2002. Red lines illustrate the azimuthal geomagnetic field gradient—continuous lines positive, dashed line—negative gradient. Stars denote the positions of neutron monitors used as data source for this analysis.

injection of plasma from the night side neutral line, which forms the storm-time ring current. This process marks the formation of storm's *main phase*, characterized by an abrupt weakening of geomagnetic field.

Due to the fact that geomagnetic storm feeds the magnetosphere with huge amount of solar plasma and energy, it was assumed that large geomagnetic storms produce enlargement of Earth's radiation belts. Such enlargement really happens during the initial storm phase, when the population of relativistic electrons could increase rapidly within a few minutes (Daglis et al., 2019). Magnetospheric compression results in a loss of some electrons through magnetopause in the interplanetary space (a process known as *magnetopause shadowing*). If the compression is large enough, the entire population of the outer radiation belt could suddenly decrease by orders of magnitude on time scale of hours—an event known as *dropout* (Borovsky & Denton, 2009; Staples et al., 2022). The resulting net electron loss extends over the main phase of geomagnetic storm, replaced later on by acceleration mechanism, recovering the pre-storm conditions.

Similar tendency is found also in the *inner* radiation belt (more precisely on its outer edge at L shell near 2) (Xu et al., 2019). During the *main* storm phase, the constancy of particles' magnetic moment is violated, when they approach the equatorial region of stretched and weakened geomagnetic field, if their gyro radius becomes comparable with the radius of geomagnetic field lines curvature. This leads to an abrupt non-adiabatic loss of *inner* radiation belt protons, because they are not able to complete their gyro-orbit before the geomagnetic field has changed its intensity—a process known as *field line curvature scattering* (Selesnick et al., 2010). With this information in mind, we are ready to understand the longitudinal heterogeneity of FD, shown in Figure 1.

When a traveling interplanetary disturbance approaches the Earth, it presses the magnetosphere and strengthens the geomagnetic field. The increased magnetic field intensity slows down the drift velocity of radiation belts' particles (refer to Equation 1), as well as the $(\mathbf{E}x\mathbf{B})/B^2$ drift. Consequently, the charge separation electric field becomes powerless, being able to expel much less of particles confined in the geomagnetic trap—particularly in regions with *positive* azimuthal gradient. This effect is detected by the ground-based neutron monitors as a sudden decrease of counting rates. While the magnetosphere is compressed, the density of trapped particles is significantly reduced, which amplifies the effect of geomagnetic strengthening.

In regions with *negative* magnetic gradient, the strongest geomagnetic field during the *initial* storm phase will severely reduce the azimuthal drift component (being reversely proportional to the third degree of magnetic field intensity). Due to the fact that in these regions the azimuthal drift has a negative sign (the first term in Equation 1), the overall drift velocity of charged particles (determined by the curvature drift) will enhance. This means that confined particles will escape easier from the magnetic trap in these regions, and a weak positive Forbush effect could be observed. This effect is well visible in ozone profiles during the initial phase of the analyzed geomagnetic storms (not shown).

During the *main* storm phase the geomagnetic field is severely weakened, and according to Equation 1 the azimuthal particles' drift significantly increased. This means that in regions with *positive* longitudinal magnetic gradient, the overall drift velocity would intensify, while in those with a *negative* gradient—it would weaken. Due to the total depletion of charged particles in radiation belts, however, the impact of this phase in the FD should be smaller. Nevertheless, it marks the beginning of the FD recovery phase.

The third FD appears in geomagnetically quiet period 31 December 2001 to 3 January 2002, and this obviously justifies the different shape of its spatial distribution (see Figure 1c). Having in mind the genesis of this type of

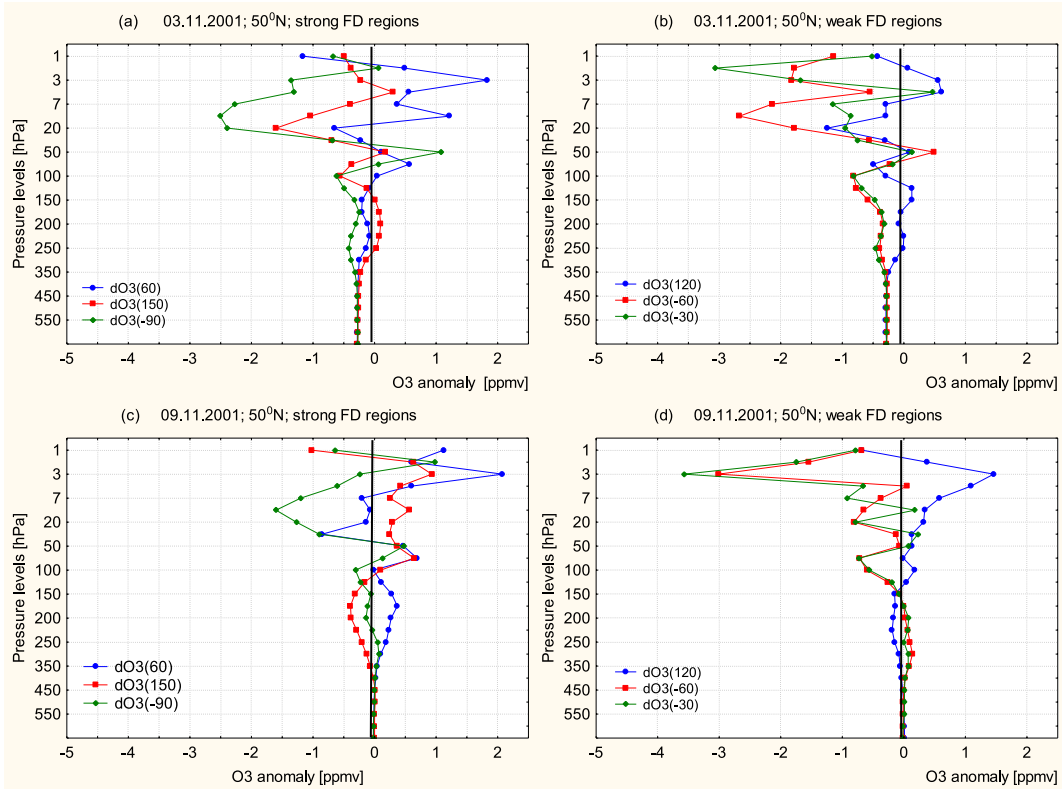

Figure 2. (a, b) Quiet ozone anomalies profiles for 1 November 2001, measured in regions with strong (a) and weak (b) Forbush decrease (FD) during the storm on 6 November 2001; (c, d) Disturbed ozone profiles *after* the geomagnetic storm on 6 November 2001, followed by FD, shown for regions of strong (c) and weak (d) depletion of galactic cosmic rays.

FDs—being a result of lateral detachment of the magnetosphere (more specifically its dusk side) by magnetic irregularities (usually corotating interaction regions)—we suggest that obtained shape of FD reflects the configuration of magnetic cloud in the near-Earth space.

3.2. Ozone Profile's Response to Geomagnetic Storms in November 2001

Previous studies have found that the total ozone's reply to geomagnetic storms is better visible at 50° northern latitude (Fedulina & Laštovička, 2001; Laštovička, J., Križan, P., 2005). So, as a first step, we have examined the quiet and disturbed ozone profiles at this latitude, comparing the effect found in regions with strong and weak FD. Based on the maps of the FDs amplitude (refer to Figure 1), we have selected the following longitudes, where a strong reduction of galactic CRs intensity has been detected: (a) 90°W, 60°E, 150°E—for the storm on 6 November 2001, and (b) 110°W, 70°W, 70°E, 150°E—for the storm on 25 November 2001. As representatives of regions with weak FD have been selected the following longitudes: (a) 60°W, 30°W, 120°E—for the first storm, and (b) 10°W, 0°E, 90°E, 120°E for the second one. Results are shown in Figures 2 and 3.

Analysis of Figures 2a and 2b reveals that before the geomagnetic storm on 6 November 2001, the lower stratospheric ozone (i.e., at 100–50 hPa levels) is slightly increased (relative to its monthly mean values), at all longitudes along the 50°N latitude. With the onset of FD, the ozone density starts gradually decreasing and on 8 and 9 November it is noticeably reduced (see Figures 2c and 2d). Similar is the ozone response to the second geomagnetic storm, but the amplitude of its reduction in the lower stratosphere is significantly higher. Thus the weak positive anomalies, visible at all longitudes before the storm onset, are turned into negative ones for 2 days after the occurrence of FD (on 25 November 2001)—refer to Figure 3.

The examination of ozone anomalies allows easier detection of changes, but the shape of ozone profile is helpful to situate the observed changes on the vertical. The changes in real ozone profile, depending on geomagnetic activity at the beginning of November 2001, are shown in Figure 4. Note the existence of well pronounced

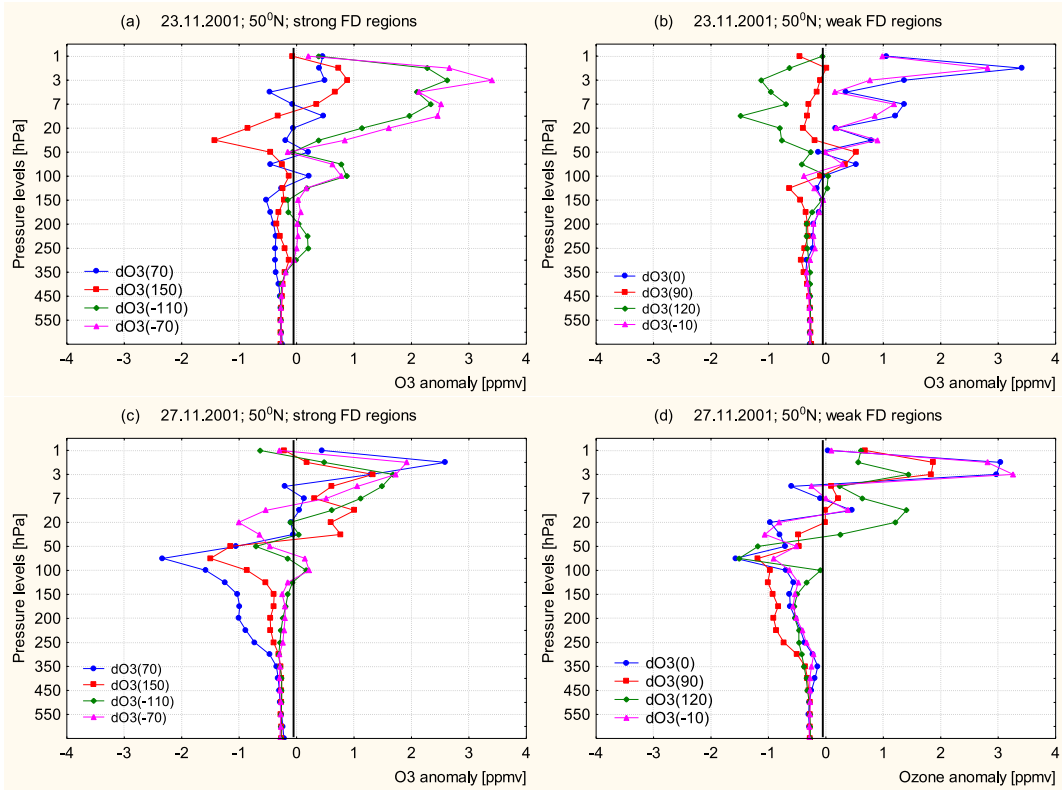

Figure 3. (a, b) Pre-storm ozone anomalies profiles for 23 November 2001, measured in regions with upcoming strong (a), and weak (b), depletion of galactic cosmic ray intensity; (c, d) Ozone profiles response to the reduced particles' flux during the geomagnetic storm on 24 November, with a Forbush decrease (FD) on 25 November 2001, in regions with strong (c), and weak (d), FD.

secondary maximum near 50 hPa in the pre-storm atmosphere, which is significantly reduced after the storm. The shape of ozone profile and its reply to the second geomagnetic storm is very similar.

The heterogeneous character of FDs illustrated in Figure 1, as well as the ozone profiles shown in Figures 2 and 3, suggests that ozone's reply to changing particles' flux intensity is also irregularly distributed over the planet. Figure 5 compares the maps of ozone anomalies at 70 hPa in pre-storm (1 and 23 November 2001), with after-storm conditions (9 and 27 November 2001). Note that the disordered distribution of ozone pre-storm anomalies appears well organized after the storms. Moreover, the centers of negative and positive ozone anomalies could be apparently attributed to the magnitude of the FD. For example, the strongest reduction of the lower stratospheric ozone over eastern Canada and Greenland, during the first storm (Figure 5b), fairly well corresponds to the region of strongest CRs depletion (refer to Figure 1a). The center of ozone enhancement over Scandinavia

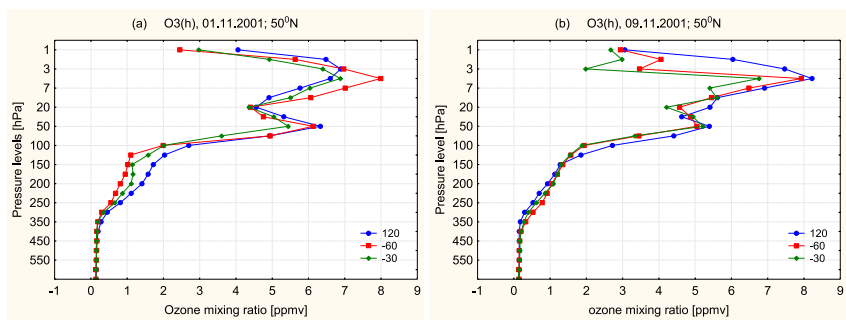

Figure 4. Comparison of ozone profiles during geomagnetically quiet (a) and disturbed conditions (b) during the storm on 6 November 2001.

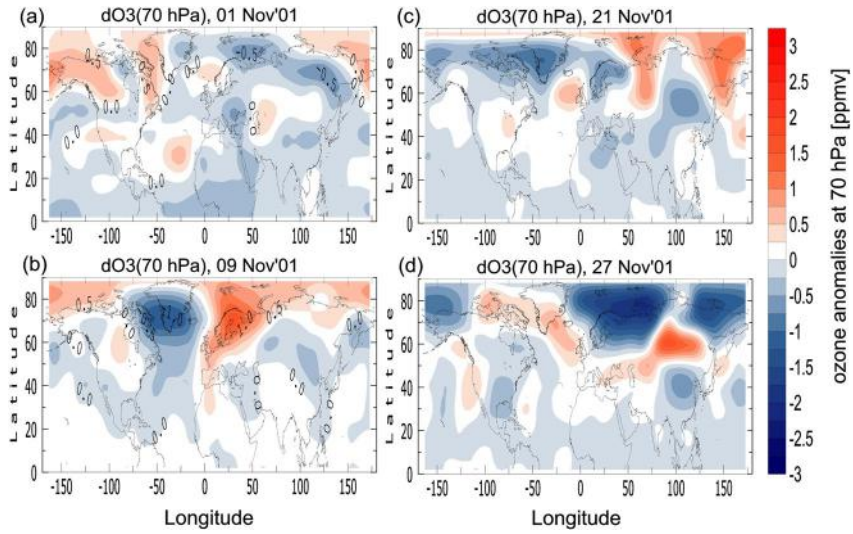

Figure 5. Maps of ozone mixing ratio anomalies at 70 hPa during pre-storm (a, c) and post-storm (b, d) conditions. Note that maximal ozone response to geomagnetic storms fairly well corresponds to the magnitude of Forbush decrease (refer to Figure 1).

could be attributed to practically unchanged particles' flux in this region, during the 6 November 2001 storm. The situation is modified to the opposite during the second storm in November 2001. The strongest ozone reduction is found over the Arctic Ocean and Scandinavia (see Figure 5d), and it could be attributed to the strongest FD, detected by the neutron monitors in this region (refer to Figure 1b). The positive ozone anomalies, found over South-Eastern Europe and central Asia, could be pertained to the weaker FD in these regions (see Figure 1b).

3.3. Ozone's Profile Response to the Period of FD (31 December 2001 to 3 January 2002)

The third analyzed event of FD is not a geomagnetic storm companion. December 2001 and January 2002 are quiet months without any geomagnetic disturbances. Anyhow, a quite strong FD appeared at the end of 2001. Its maximal effect is detected by the neutron monitors' network in various days during the period 31 December 2001 to 3 January 2002. According to Oh et al. (2008), the presence of such non-simultaneous (in universal time) FDs must be attributed to the magnetic irregularities, propagating laterally from the Sun-Earth direction, which hit the Earth's magnetosphere on its dusk side. This event has been chosen in attempt for differentiation between ozone's responses to geomagnetic storms (with their complex impact on the upper atmosphere), and decreased CRs intensity due to the Forbush effect.

Figure 6 illustrates the differences between ozone profiles before (30 December 2001) and after (5 January 2002) the FD, separately for regions with strongly and weakly depleted CRs. Similarly to the coupled magnetic storm-FD events, the ozone density is significantly reduced during this unrelated to geomagnetic disturbance FD—particularly in regions with strong reduction of CRs' intensity, between 3 and 150 hPa (Figure 6a). Oppositely, in regions with weak particles' decrease, the ozone density is slightly enhanced (Figure 6b).

An idea about the spatial distribution of ozone anomalies at 70 hPa (i.e., deviations from its monthly mean values) is given in Figure 7. Note that the region of strongest ozone reduction (over the North Atlantic) fairly well corresponds to the region of strongest FD (refer to Figure 1). This result indicates that changes of ozone density, obtained during the geomagnetic storms, are apparently related to the reduced particles' flux reaching the lower atmosphere.

3.4. Relations Between Lower Stratospheric Ozone and Sea Level Pressure

Some authors have noticed that after strong geomagnetic disturbances, the surface pressure significantly drops (Avakyan et al., 2015; Bucha, 1991; Danilov & Lastovicka, 2001; Mustel et al., 1977). For example, Mustel et al. (1977) have noticed that in the latitudinal belt 47°–75°N the surface pressure decreases by about 2 mbar,

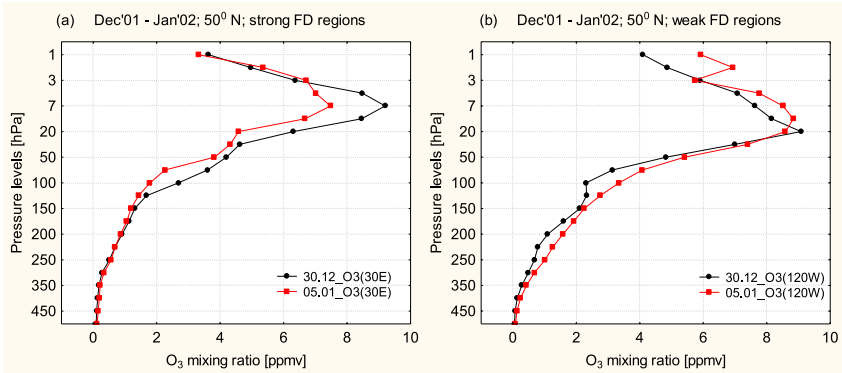

Figure 6. Comparison of ozone mixing ratio profiles before and after the prolonged Forbush decrease (FD) within the period 31 December 2001 to 3 January 2002; (a) in regions with strong FD, and (b) in regions with weak FD.

following strong geomagnetic disturbances. Later on Laštovička and Mlch (1999) pointed out that tropospheric pressure and temperature, as well as the total ozone density, are highly sensitive to geomagnetic storms in two main regions: North Atlantic—Europe and Siberia—Aleutian islands. These results were our motivation to compare the spatial distribution of ozone anomalies at 70 hPa with the sea level pressure, before and after the FD.

Figure 8 compares the spatial distribution of ozone changes (due to the reduced CRs' intensity) with the map of sea level pressure anomalies (i.e., its deviations from monthly mean values). The maximal effect of CRs' depletion on the ozone density at 70 hPa has been found for 2–3 days after the onset of FDs. The synchronization between ozone and the sea level pressure could be tracked since that dates, but the best similarity has been found for 3–4 days after the maximization of the FD's effect on the ozone. The coincidence of the spatial allocation of positive ozone anomalies and the negative ones in the sea level pressure, and vice versa, is really impressive. Note that the relation is not a rigid, but depends on the sign of ozone changes. The latter, on its turn, is determined by the amount of energetic particles reaching the lower atmosphere (Kilifarska, 2013). Thus, the severe decrease of particles' flux is projected as a negative ozone anomaly in the lower stratosphere, while the small or positive changes—as neutral or positive ones.

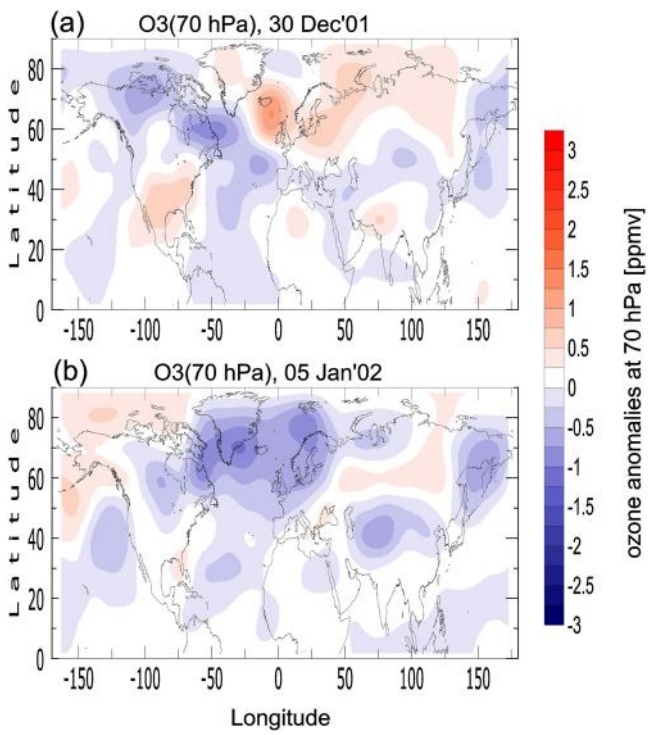

Figure 7. (a) Spatial distribution of ozone anomalies at 70 hPa before the Forbush decrease (within the period 1 December 2001 to 3 January 2002), and after that (b).

Finally, we have compared the spatial distributions of ozone at 70 hPa and sea level pressure, during the third FD (Figure 9). The figure illustrates the temporal evolution of changes in both fields and a consecutive adaptation of pressure to the ozone changes. For example, on the first day of FD (31 December 2001) there is some similarity between ozone and pressure spatial distributions, but it is far from the synchronization. With progression of FDs, the negative ozone anomaly—initially detected over the North-Eastern Canada—is moved eastward, covering the Greenland, Island, and North Atlantic up to Scandinavia (3 January 2002). At the same time, the sea level pressure anomalies are reformed—from diffusive positive anomalies over the North-Western America, Greenland, and Arctic, to the well-defined center of positive anomaly—located over North Atlantic and Scandinavia. On 5 January 2002, when the ozone negative anomaly has reached its maximal size, the pressure anomaly is expanded northward, corresponding fairly well to the shape of the negative ozone anomaly (see Figure 9).

In resume, the analysis of ozone response to different types of FDs reveals that ozone density in the lower stratosphere follows the intensity of particles' fluxes penetrating in Earth's lower atmosphere. In accordance with previous studies, we have found that FDs are accompanied by corresponding changes of the sea level pressure. We attribute these pressure changes to relevant

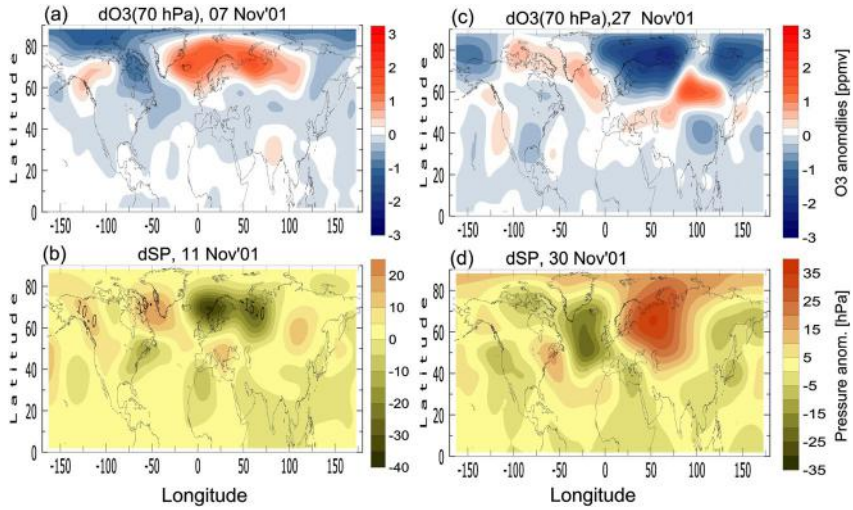

Figure 8. Maps of ozone and sea level pressure deviations (from their monthly means) after the geomagnetic storms with Forbush decreases (FDs) on 6 November 2001 (a, b) and 24 November 2001 (c, d). Note the good correspondence between ozone anomalies (found for 2 days after the FD onset) and pressure anomalies, obtained for 3–4 days after the ozone changes.

variations in the lower stratospheric ozone density. The physical mechanism connecting ozone's density with the sea level pressure will be described in the following subsection.

3.5. Mechanism of Ozone Influence on the Surface Atmospheric Pressure

The lower stratospheric ozone is able to influence the sea level pressure in two different ways—*direct* and *indirect*. The *direct* mechanism consists of local changes of atmospheric pressure in the lower stratosphere, due to the ozone's capacity to absorb the incoming solar radiation. Thus, the rise of ozone and consequent warming of the lower stratosphere reduces the local atmospheric pressure, due to the increased diffusion velocity of atmospheric molecules. Ozone depletion, on the other hand, cools the atmosphere, reduces the mobility of atmospheric constituents, followed by enhancement of the local atmospheric pressure. The changes of stratospheric pressure are projected on the sea-level one, which itself is an integral characteristic of the whole atmospheric columnar weight above the sea surface.

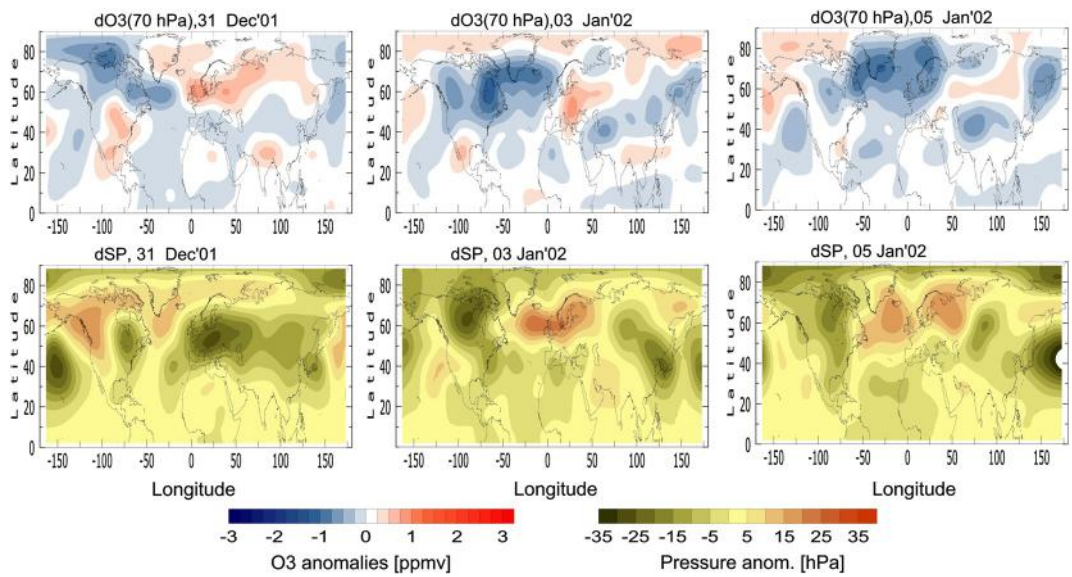

Figure 9. Temporal evolution of ozone deviations (from its monthly means) during and after Forbush decrease (top panels), and sea level pressure anomalies (bottom panels).

The *indirect* mechanism of the lower stratospheric distant influence on the sea level pressure, consists of a link of relations between atmospheric variables. As noted above, the ozone variations alter the temperature in the near tropopause region and the static stability of the upper troposphere (North & Eruhimova, 2009; Young, 2003). Thus, the tropopause warming stabilizes the atmosphere, leading to its gradual drying—due to the reduced upwelling of moisture, transported from the lower wetter atmospheric layers. Taking into account that 90% of the greenhouse power of the whole water vapor available in the atmosphere is determined by the upper tropospheric vapor (Inamdar et al., 2004; Sinha & Harries, 1995; Spencer & Braswell, 1997), it becomes clear that ozone enhancement forces a cooling of the near-surface air temperature (Kilifarska, 2013; Kilifarska et al., 2020). Oppositely, a reduction of the lower stratospheric ozone density cools the tropopause and destabilizes the upper troposphere. This enables vertical motions, which moisten the upper troposphere. The greenhouse effect of the wetter upper troposphere is much stronger, and raises the near-surface air temperature.

Analysis of Figures 8 and 9 shows that the greatest ozone and pressure anomalies related to the FDs are visible in the latitudinal band 50°–70°N. Our previous analyses (Kilifarska, Bakhmutov, & Melnyk, 2022) reveal that at these latitudes is detected a centennial enhancement of ozone at 70 hPa between the first decades of 20 and 21st centuries. The strongest ozone impact on the sea level pressure, within the period 1900–2019, is found exactly in the same region (Kilifarska, Velichkova, & Mokreva, 2022). This suggests that the most probable mechanism of ozone influence on the sea level pressure near 50° latitude is the *direct* one.

4. Discussion

The lower stratospheric ozone's impact in the variations of the near-surface temperature and pressure, at various time scales, is not well understood. Although the mechanism of near tropopause ozone influence is built up into the climatic models, it actually is not explored in the contemporary climatic modeling, because of inaccurate understanding of the factors effecting ozone variability at these levels. Thus, the additional source of ozone production in the lower stratosphere (Kilifarska, 2013) is completely ignored by climatic modelers. As a result, the comparison with measurements is more than unsatisfactory—showing models' inability to describe neither the climatic hiatus (observed in the first decade of 21st century), nor the regionality of climate change, and particularly the climatic modes.

The examination of ozone profile's response to the changing intensity of energetic particles, precipitating in the lower atmosphere, reveals its certain response. We show that the strongest depletion of the lower stratospheric ozone density is found in regions with strongest FD, with a time delay of 2–3 days. Although the impact of the reduced particles' flux on the ozone profiles is illustrated for 50° latitude, the effect is well visible at lower latitudes as well (although with a smaller magnitude). This result confirms the validity of our concept about the existence of additional source of ozone in the lower stratosphere, which is significantly dumped in periods with decreased CRs intensity.

The comparison of ozone and pressure anomalies, in relation to FDs, confirms the results reported previously about an abrupt depletion of surface pressure found after strong geomagnetic storms (Avakyan et al., 2015; Bucha, 1991; Danilov & Lastovicka, 2001; Mustel et al., 1977). We illustrate that ozone-pressure changes are well synchronized, and this synchronization is achieved through a dynamical adaptation of the sea level pressure to changes in the lower stratospheric ozone. The pressure reply is delayed by 2–4 days and this short delay implies that the observed changes are more likely due to the local changes of temperature and pressure, at the level of ozone variations. This study shows the importance of the lower stratospheric ozone variability for understanding the spatial-temporal variations of the near-surface pressure.

5. Conclusions

This analysis throws some more light on the lower stratospheric ozone response to the decrease of CRs intensity, reaching the lower atmospheric levels. We show that reduced particles' flux is the most probable reason for changes in ozone profile beneath the ozone's maximum. The time delay of ozone response is 1–3 days which certainly implies that observed ozone changes could not be attributed to significantly slower stratospheric circulation. Moreover, the changes in ozone profile are well traceable at subtropical latitudes, which is an additional argument against the circulation impact.

Analysis of the spatial distribution of the sea-level pressure and ozone anomalies reveal that they are well synchronized within 2–4 days after the onset of FD. Examination of their temporal evolution shows that pressure anomalies dynamically respond to changes in the ozone density at 70 hPa.

The presented results confirm our assumptions that: (a) variability of the lower stratospheric ozone is strongly dependent on the intensity of CRs penetrating the lower stratosphere; (b) sea-level pressure is tightly connected to the spatial-temporal variations of the ozone in the lower stratosphere.

Data Availability Statement

Access to ERA-Interim data are deactivated since 1 June 2023, but ECNWF provides an updated reanalysis ERA 5 (https://registry.opendata.aws/ecmwf-era5), where atmospheric ozone and sea level pressure could be retrieved from (registration is required). Data for cosmic rays flux, measured at the ground surface, are freely available at https://www.nmdb.eu/nest/ and http://cr0.izmiran.ru/common/links.htm. Graphs of ozone profiles are created by the use of the STATISTICA commercial software (StatSoft's license). Maps are created by the use of the SURFER program, license held by the Golden Software.

Acknowledgments
The authors are thankful to the project teams of ERA-Interim reanalysis, for providing gridded data for ozone temperature and pressure. The authors acknowledge the NMDB database (www.nmdb.eu), founded under the European Union's FP7 program (contract no. 213007), as well as the IZMIRAN neutron monitors database (http://cr0.izmiran.ru/common/links.htm) for the data provided. This research was funded by the National Science Fund of Bulgaria (contract KP-06-N34/1/30-09-2020).

References

Avakyan, S. V., Voronin, N. A., & Nikolsky, G. A. (2015). Response of atmospheric pressure and air temperature to the solar events in October 2003. *Geomagnetism and Aeronomy*, *55*(8), 1180–1185. https://doi.org/10.1134/S0016793215080034

Bekoryukov, V. I., Bugaeva, I. V., Purgansky, V. S., Ryazanova, A. A., & Starodubcev, V. A. (1976). On the relation of upper atmospheric processes to solar activity. *Proceedings of studies of dynamical processes in the upper atmosphere* (pp. 5–l8). Gidrometeoizdat.

Belinskaya, A., Kazimirovsky, E., Matafonov, G., & Sych, R. (2001). The regional peculiarities of the total ozone content variations caused by solar/geomagnetic phenomena. *Advances in Space Research*, *27*(12), 2007–2011. https://doi.org/10.1016/S0273-1177(01)00306-4

Belov, A. V., Eroshenko, E. A., Yanke, V. G., Oleneva, V. A., Abunina, M. A., & Abunin, A. A. (2018). Global survey method for the world network of neutron monitors. *Geomagnetism and Aeronomy*, *58*(3), 356–372. https://doi.org/10.1134/S0016793218030039

Bhargawa, A., Yakub, M., & Singh, A. K. (2019). Repercussions of solar high energy protons on ozone layer during super storms. *Research in Astronomy and Astrophysics*, *19*(1), 002. https://doi.org/10.1088/1674-4527/19/1/2

Borovsky, J. E., & Denton, M. H. (2009). Relativistic-electron dropouts and recovery: A superposed epoch study of the magnetosphere and the solar wind. *Journal of Geophysical Research*, *114*(A2), A02201. https://doi.org/10.1029/2008JA013128

Bucha, V. (1991). Solar and geomagnetic variability and changes of weather and climate. *Journal of Atmospheric and Terrestrial Physics, The 7th International SCOSTEP symposium on Solar-Terrestrial Physics*, *53*(11–12), 1161–1172. https://doi.org/10.1016/0021-9169(91)90067-H

Bucha, V., & Bucha, V. (1998). Geomagnetic forcing of changes in climate and in the atmospheric circulation. *Journal of Atmospheric and Solar-Terrestrial Physics*, *60*(2), 145–169. https://doi.org/10.1016/S1364-6826(97)00119-3

Daglis, I. A., Katsavrias, C., & Georgiou, M. (2019). From solar sneezing to killer electrons: Outer radiation belt response to solar eruptions. *Philosophical Transactions of the Royal Society A*, *377*(2148), 20180097. https://doi.org/10.1098/rsta.2018.0097

Danilov, A. D., & Laštovička, J. (2001). Effects of geomagnetic storms on the ionosphere and atmosphere. *International Journal of Geomagnetism and Aeronomy*, *2*(3), 209–224.

Fedulina, I. N. (1998). Changes of ozone content at middle latitudes during Forbush decreases in cosmic rays. *Studia Geophysica et Geodaetica*, *42*(4), 521–532. https://doi.org/10.1023/A:1023301322428

Fedulina, I., & Laštovička, J. (2001). Effect of Forbush decreases of cosmic ray flux on ozone at higher middle latitudes. *Advances in Space Research*, *27*(12), 2003–2006. https://doi.org/10.1016/S0273-1177(01)00303-9

Inamdar, A. K., Ramanathan, V., & Loeb, N. G. (2004). Satellite observations of the water vapor greenhouse effect and column longwave cooling rates: Relative roles of the continuum and vibration-rotation to pure rotation bands. *Journal of Geophysical Research*, *109*(D6), D06104. https://doi.org/10.1029/2003JD003980

Kilifarska, N. A. (2013). An autocatalytic cycle for ozone production in the lower stratosphere initiated by Galactic Cosmic rays. *Comptes rendus de l'Academie bulgare des Sciences*, *66*(2), 243–252. https://doi.org/10.7546/cr-2013-66-2-13101331-12

Kilifarska, N. A., Bakhmutov, V. G., & Melnyk, G. V. (2020). *The hidden link between Earth's magnetic field and climate*. Elsevier. https://doi.org/10.1016/C2018-0-01667-9

Kilifarska, N. A., Bakhmutov, V. G., & Melnyk, G. V. (2022). Coupling between geomagnetic field and Earth's climate system. In K. S. Essa, K. H. Mahmoud, & Y.-H. Chemin (Eds.), *Magnetosphere and solar winds, humans and communication* (pp. 11–36). IntechOpen.

Kilifarska, N., Velichkova, T., & Mokreva, A. (2022). North Atlantic Oscillation and variations of the total geomagnetic field intensity. *Comptes rendus de l'Academie bulgare des Sciences*, *75*(11), 1628–1637. https://doi.org/10.7546/CRABS.2022.11.10

Laštovička, J., & Križan, P. (2005). Geomagnetic storms, Forbush decreases of cosmic rays and total ozone at northern higher middle latitudes. *Journal of Atmospheric and Solar-Terrestrial Physics, Solar Activity Forcing of the Middle Atmosphere*, *67*(1–2), 119–124. https://doi.org/10.1016/j.jastp.2004.07.021

Laštovička, J., & Mlch, P. (1999). Is ozone affected by geomagnetic storms? *Advances in Space Research*, *24*(5), 631–640. https://doi.org/10.1016/s0273-1177(99)80136-7

Mustel, E. R., Chernoprud, V. E., & Khvedeliani, V. A. (1977). Comparison of variations in surface atmospheric pressure field in periods of high and low geomagnetic activity. *Astronomicheskii Zhurnal*, *54*, 682–697.

North, G. R., & Eruhimova, T. L. (2009). *Atmospheric thermodynamics: Elementary physics and chemistry*. Cambridge University Press.

Oh, S. Y., & Yi, Y. (2009). Statistical reality of globally nonsimultaneous Forbush decrease events. *Journal of Geophysical Research: Space Physics*, *114*(A11), A11102. https://doi.org/10.1029/2009JA014190

Oh, S. Y., Yi, Y., & Kim, Y. H. (2008). Globally nonsimultaneous Forbush decrease events and their implications. *Journal of Geophysical Research: Space Physics*, *113*(A1), A01103. https://doi.org/10.1029/2007JA012333

Okoro, E. C., Okoh, D. I., Okeke, F. N., & Anoruo, C. M. (2022). Relationship between variation of total ozone concentration and severe geomagnetic storms over Lagos in Nigeria. *British Journal of Earth Sciences Research*, *10*(2), 39–54.

Selesnick, R. S., Hudson, M. K., & Kress, B. T. (2010). Injection and loss of inner radiation belt protons during solar proton events and magnetic storms. *Journal of Geophysical Research*, *115*(A8), A08211. https://doi.org/10.1029/2010JA015247

Shirochkov, A. V., & Nagurny, A. P. (1992). On the problem of a connection between the ozone dynamics at high latitudes and magnetospheric processes. *Journal of Atmospheric and Solar-Terrestrial Physics*, *54*(7–8), 835–840. https://doi.org/10.1016/0021-9169(92)90049-Q

Simmons, A., Uppala, S., Dee, D., & Kobayashi, S. (2006). ERA-Interim: New ECMWF reanalysis products from 1989 onwards. [Dataset]. ECMWF Newsletter, *110*, 26–35. https://doi.org/10.21957/pocnex23c6

Sinha, A., & Harries, J. E. (1995). Water vapour and greenhouse trapping: The role of far infrared absorption. *Geophysical Research Letters*, *22*(16), 2147–2150. https://doi.org/10.1029/95GL01891

Spencer, R. W., & Braswell, W. D. (1997). How dry is the tropical free troposphere? Implications for global warming theory. *Bulletin of the American Meteorological Society*, *78*(6), 1097–1106. https://doi.org/10.1175/1520-0477(1997)078<1097:HDITTF>2.0.CO;2

Staples, F. A., Kellerman, A., Murphy, K. R., Rae, I. J., Sandhu, J. K., & Forsyth, C. (2022). Resolving magnetopause shadowing using multi-mission measurements of phase space density. *Journal of Geophysical Research: Space Physics*, *127*(2), e2021JA029298. https://doi.org/10.1029/2021JA029298

Storini, M. (2001). Geomagnetic storm effects on the Earth's ozone layer. *Advances in Space Research*, *27*(12), 1965–1974. https://doi.org/10.1016/S0273-1177(01)00284-8

Tassev, Y., Velinov, P. I. Y., Mateev, L., & Tomova, D. A. (2003). Comparison between effects of solar proton events and of geomagnetic storms on the ozone profiles. *Advances in Space Research*, *31*(9), 2163–2168. https://doi.org/10.1016/s0273-1177(03)00126-1

Veretenenko, S., & Ogurtsov, M. (2012). Regional and temporal variability of solar activity and galactic cosmic ray effects on the lower atmosphere circulation. *Advances in Space Research*, *49*(4), 770–783. https://doi.org/10.1016/j.asr.2011.11.020

Xu, J., He, Z., Baker, D. N., Roth, I., Wang, C., Kanekal, S. G., et al. (2019). Characteristics of high-energy proton responses to geomagnetic activities in the inner radiation belt observed by the RBSP satellite. *Journal of Geophysical Research: Space Physics*, *124*(9), 7581–7591. https://doi.org/10.1029/2018JA026205

Young, J. A. (2003). Static stability. In R. Holton, J. A. Curry, & J. A. Pyle (Eds.), *Encyclopaedia of atmospheric sciences* (Vol. 2, pp. 423–430). Academic Press.